



Features of highly sensitive thermoluminescence dosimetry $\text{Ag}_3\text{PO}_4:\text{Li}$ nanophosphor under gamma irradiation

A. Hussein¹, E. R. Sheha^{2,a} , A. El-Adawy¹, S. Abdel-Samad², Ahmad A. Hassan³, M. Al-Abyad²

¹ Physics Department, Faculty of Science, Menoufia University, Menoufia, Egypt

² Cyclotron Facility, Nuclear Physics Department, Nuclear Research Center, Egyptian Atomic Energy Authority, Cairo 13759, Egypt

³ Metallurgy Department, Nuclear Research Center, Egyptian Atomic Energy Authority, Cairo 13759, Egypt

Received: 21 October 2021 / Accepted: 15 April 2022

© The Author(s) 2022

Abstract In this work, new synthetic nanophosphor materials of Li^+ doped Ag_3PO_4 orthophosphate were prepared with different impurity concentrations. The coprecipitation method was utilized in the preparation at room temperature. The prepared nanophosphors were characterized via x-ray diffraction and high-resolution transmission electron microscopy, and the results confirmed the existence of nanoparticles. The thermoluminescence properties of samples with different concentrations of Li-cohost salt were extensively studied. The Ag_3PO_4 sample doped with 5 Wt% of Li (i.e. APL_5) impurity revealed the highest thermoluminescence intensity of any of the other compositions, according to the thermoluminescence response of the synthesized nanophosphors. All the studied samples were subjected to optimum thermal annealing of 500 °C for 1 h and readout with thermoluminescence reader at a heating rate of 5 °C/s. The APL_5 nanophosphor samples revealed a good linearity dependence of thermoluminescence response against gamma dose within the range of 15–100 Gy. This sample showed a relatively low rate of fading of about 19% within two months of storage and good reusability. These characteristics make the newly prepared APL_5 phosphor highly considered as a new potential thermoluminescence dosimeter and can be efficiently used in various γ -radiation detection applications.

1 Introduction

Thermoluminescent dosimeters (TLD) are passive dosimeters commonly used to provide the total cumulative dose due to radiation exposure. The growing need for highly sensitive, good quality new dosimeters has led to many appreciable research studies [1]. During the last decades, there has been extensive research on the use of thermoluminescence detectors (TLDs) in the field of radiation dosimetry. Worldwide, there are different types of phosphor-based thermoluminescent dosimetric families widely in use [2]. Thermoluminescence (TL) materials are made up of bulk, micro, and nanocrystal structures, with the latter having more favorable TL properties than the others [3, 4].

Dosimeters have a wide range of successful applications in radiation monitoring, including environmental and personal exposure [5]. The TL phenomenon in a given material is a thermally stimulated light emission that follows a previous absorption of energy from radiation. [6]. When a sensitive photomultiplier tube detects the released optical photons (luminescence spectrum), a pulse height spectrum known as a glow curve is produced. The presence of trapping states in the detector materials is closely related to the shape of the glow curve, peaks position, and TL-intensity [7, 8]. Recently, orthophosphates including LiMgPO_4 , LiBaPO_4 , LiCaPO_4 , and Li_3PO_4 phosphors have found increasing interest for their potential applications in the field of scintillators, solid-state lighting, and TLDs [9–12]. In addition, this was referred to as their good features such as high emission intensity, nontoxicity, good luminescent properties, low-cost synthesis method, and excellent thermal stability [13–15]. Currently, silver orthophosphate (Ag_3PO_4) is an important host material for activator ions in their lattice according to, its high chemical stability, higher quantum yield, and low sintering temperature [16–26]. Moreover, it has become a promising photocatalyst driven by visible light. Therefore, the progress of studying the Ag_3PO_4 -based dosimetry will be one of the focus of this work.

The work presented herein was intended to synthesize and investigate the thermoluminescence properties of new, inexpensive nanostructure systems of undoped Ag_3PO_4 and lithium doped silver orthophosphate (APL) compounds. Furthermore, the effects of the Li-cohost salt type, Li^+ dopant concentrations, and conditions of annealing on the TL characterizations of these synthesized samples were extensively studied to explore the possible use of such new prepared compounds as promising gamma dosimeter.

^a e-mail: emad.sheha@eaea.org.eg (corresponding author)

2 Materials and methods

2.1 Samples preparation

High purity AgNO_3 (99.98%), Na_2HPO_4 (99.98%), LiCl (99.99%), LiOH (99.98%), LiNO_3 (99.99%) and absolute ethanol were used to fabricate the undoped and Li-doped Ag_3PO_4 nanophosphor compounds.

The Ag_3PO_4 nanoparticles (NPs) sample was synthesized by the coprecipitation method [27, 28]. The preparation was carried out through the following steps: a mass of 0.5 gm of (AgNO_3) salt was dissolved completely in 50 ml of ethanol with stirring at room temperature. Then an equal amount of 0.2 M Na_2HPO_4 solution was added slowly to the previous solution under continuous magnetic stirring. As a result, a yellow precipitate was obtained and washed three times with distilled (DI) water. The precipitate was then, dried at 90 °C in an oven for 12 h to finally obtain the Ag_3PO_4 (AP) nanocrystalline sample to be ready for any further investigation.

The Li^+ doped Ag_3PO_4 (APL) nanocrystalline were synthesized at room temperature utilizing an environmentally friendly coprecipitation technique [29–31]. Through the following steps; different weight ratios of Li^+ salt (1, 3, 5, and 7 Wt%) and donated as (APL₁, APL₃, APL₅, and APL₇%), were dissolved completely in 50 ml of ethanol with stirring at room temperature. Then Li^+ salts with different concentrations were added dropwise to the previously prepared solution (AP) under stirring at room temperature. After that, the white precipitate was collected and washed with DI water to remove any organic residues. As result, a white precipitate was dried at 90 °C in an oven 12 h to finally obtain the (APL) nanoparticles sample to be ready for any further investigation.

2.2 Samples irradiation and measurement

The samples were irradiated with different gamma doses in a CM-20 gamma irradiation cell using a Co-60 source at the Cyclotron facility in Cairo, Egypt. The gamma irradiator consists of two shielded cylindrical chambers with rotating base with one opening window facing the irradiation source for each chamber. The irradiator's dose rate during irradiation was 8.11 Gy/min at room temperature. The powdered samples were placed in Ependorf tubes inside one of the irradiation chambers, at a position located along the longitudinal axis to the sources.

The X-ray diffraction (XRD) pattern of the new synthesized (AP) and (APL₅) nanostructure samples were obtained using an X-ray diffractometer, Panalytical (XPERT PRO MPD) [32], with Ni filter and Cu-K α radiation ($\lambda = 1.542 \text{ \AA}$). X-ray tube was operated at 40 kV and 30 mA anode current. The two theta degree sweep angles varied in the range $20^\circ < 2\theta > 80^\circ$ at steps of 0.02 degrees. The obtained (XRD) pattern was compared with the *Joint Council Powder Diffraction Data* (JCDPs) [33] for standards. The nanostructures of the prepared (AP) and (APL₅) phosphors were investigated using a high-resolution transmission electron microscope (HR-TEM model JEM-2100, JEOL, Japan) [34] microscope.

The thermoluminescence measurements of these γ -irradiated phosphors were carried out using Nucleonix TLD reader model 1009I [35], at NRC, EAEA. All the samples were annealed at 500 °C for 1 h before any measurements, and the readout of all samples was performed at a linear heating rate of 5 °C/s and preheating of 20 °C until reaching a maximum temperature up to 350 °C.

3 Results and discussion

3.1 Powder XRD analysis

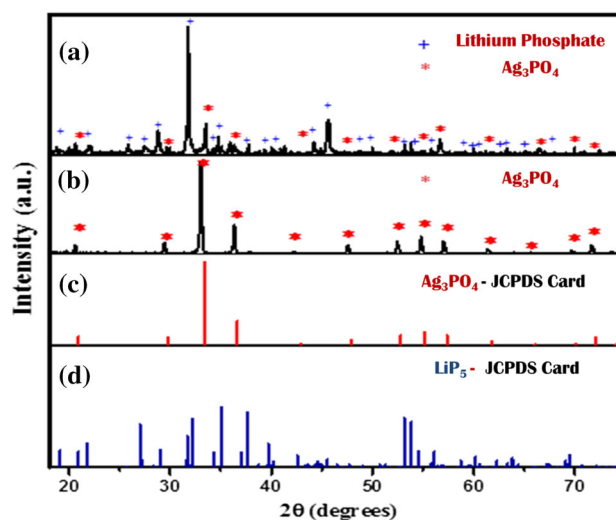
The crystalline structure and phase composition of the as-synthesized [AP and APL₅] nanocrystalline samples were confirmed by the XRD pattern as shown in Fig. 1. The pure (AP) sample exhibited the main peaks at [20.37°, 29.32°, 32.90°, 36.25°, 47.89°, 52.37°, and 54.60°] which corresponds to plans (110), (200), (210),(211), (220),(310) and (222), that indexed to the pure body-centered cubic structure of (AP) according to the standard spectrum JCPDS No. (01–089-7399) as shown in Fig.1b, c.

In addition, the XRD patterns of the Li^+ doped orthophosphate Ag_3PO_4 nanocrystalline phosphor are shown in Fig.1a, d. The diffraction peaks at 2θ positions [18.94°, 21.73°, 27.06°, 28.98°, 31.51°, 35.02°, 37.01°, 37.55°, 39.86°, 53.25°, and 53.91°] of the synthesized material were indexed by comparing them with the standard data available JCPDS No. (00–013-0282). Results confirmed the successful synthesis of highly crystalline APL₅ nanophosphor material without observing other impurity diffraction peaks.

3.2 HR-TEM analysis

Figure 2 shows the morphological characterizations of the pure Ag_3PO_4 and $\text{Ag}_3\text{PO}_4:\text{Li}^+$ investigated by the HR-TEM technique. Figure 2a exhibits the representative TEM micrograph of pure (AP) nanoparticles (NPs), with a uniform size of about 10 nm. Figure 2b depicts a TEM image that confirmed the successful preparation of (APL₅) nanocompounds (NCs), by homogenous coprecipitations method, with an average size in the range of 12–15 nm.

Fig. 1 (a) The powdered X-ray diffraction patterns of APL₅ (b) undoped Ag₃PO₄ (AP), (c) Ag₃PO₄—JCPDS card and (d) LiP₅—JCPDS card



The TEM images in Fig. 2c, d) show that all of the fine nanoparticles in the sphere exhibit clear lattice fringes with a spacing (d) of 0.12 and 0.38 nm for the Ag₃PO₄ and Ag₃PO₄:Li⁺ samples, respectively. This is considered in good agreement with the spacing of (220) and (200) planes of the cubic silver orthophosphate that confirmed the doping of Ag₃PO₄ with Li⁺ ions. The corresponding *selected area electron diffraction* (SAED) images in Fig. 2e, f) display a spot pattern for (AP) NPs that indicated a single crystalline phase and a ring pattern for (APL₅) which showed a polycrystalline phase.

3.3 Thermoluminescence measurements

First of all, the pre-annealed (500 °C for 1 h), 100 Gy gamma irradiated nanostructure of Ag₃PO₄ (AP) showed no TL response. Thereafter, the TL measurements of Ag₃PO₄:Li⁺ (APL) were extensively studied under different conditions. A detailed study will be followed up:

3.3.1 Optimum co-host type of Li salt

Three co-host types of Li salts (LiNO₃, LiOH, and LiCl) were used individually in the preparation of APL nanophosphors samples. The three samples were first annealed at 500 °C for 1 h, exposed to 100 Gy of γ -dose, and their TL-glow curves were obtained at 5 °C/s heating rate, as can be seen in Fig. 3A.

From the figure, we can notice that the shape of the glow curve, peak positions, and TL intensity is highly co-hosted depending salt type. In comparison to the other samples, the APL nanostructure prepared from LiCl salt has the highest TL intensity than the other prepared samples.

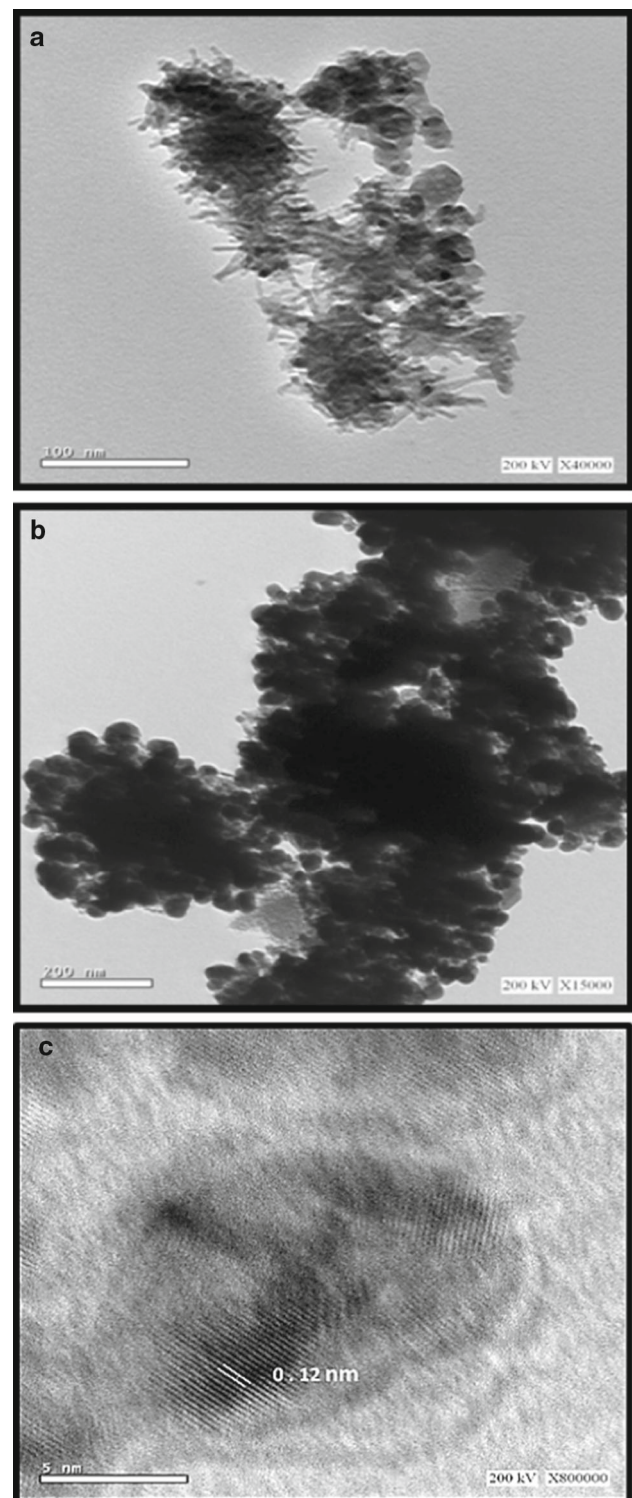
Figure 3B depicts a representation of TL-intensity values from glow curves shown in Fig. 3A, where the TL-intensity value of the APL sample prepared from LiCl co-host salt is approximately 13 and 60 times higher than that obtained from LiOH and LiNO₃ salts, respectively. As a result, we will only be interested in the APL nanostructure sample that was previously prepared using LiCl salt.

3.3.2 Optimum Li⁺ dopant concentration in APL nanophosphors

New nanophosphors made of AP nanostructure samples doped with different Li⁺ weight ratios (1, 3, 5, 6, and 7%) were prepared and donated by APL₁, APL₃, APL₅, APL₆, and APL₇, respectively. A coprecipitation approach was used in the preparation with the LiCl co-host salt. After 1 h of annealing at 500 °C, all samples were subjected to 100 Gy of γ -dose. Figure 4A shows the resulting glow curves of APL₁, APL₃, APL₅, APL₆, and APL₇ samples that were recorded at a 5 °C/s heating rate.

Figure 4A shows the resulting glow curves of Ag₃PO₄:Li⁺ samples at five different Li⁺ concentrations, with the highest TL-response corresponding to 5Wt% of Li⁺ concentration [see also representations of the TL-intensity given in Fig. 4B]. The TL-response of APL₅ was approximately 102.6, 2, 3, and 7 times higher than that of APL₁, APL₃, APL₆, and APL₇ samples, respectively, as shown in Fig. 4B. The decrease in TL-response after the optimum value of Li⁺ (i.e. 5Wt%) can be attributed to the phenomenon of concentration quenching effect [36, 37]. Therefore, only the nanophosphor sample APL₅ prepared with LiCl co-host salt will be of interest.

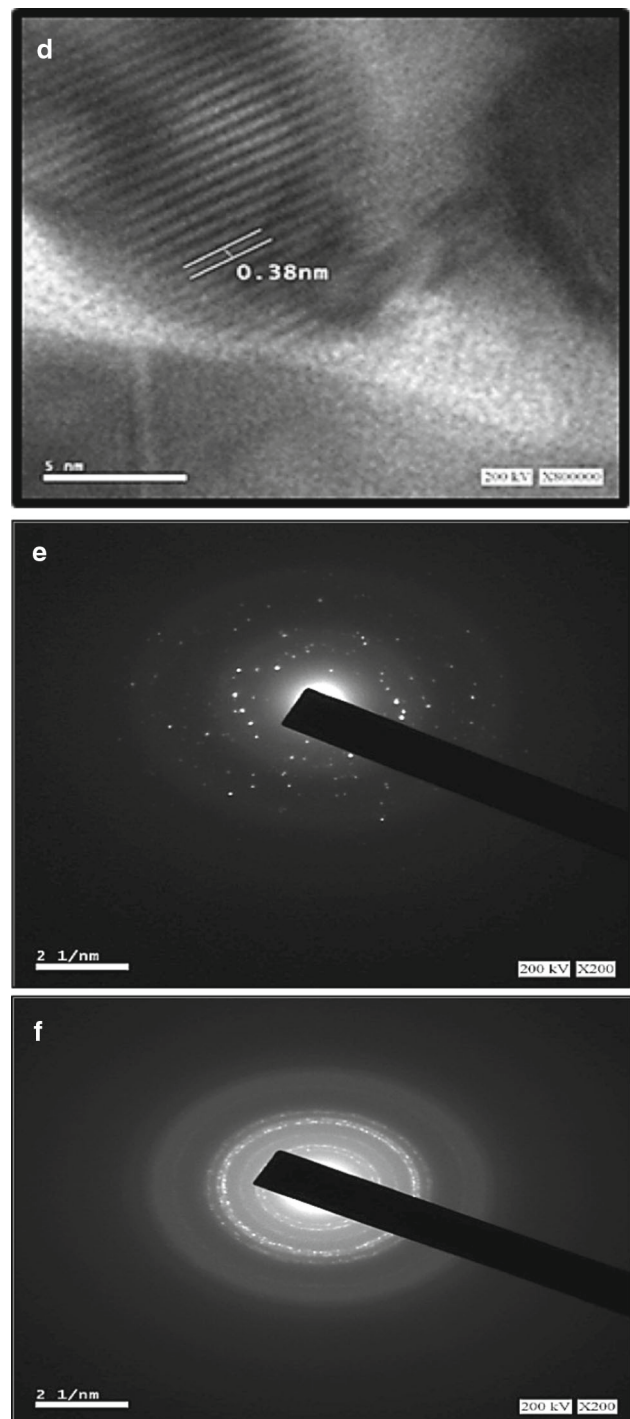
Fig. 2 (a, b) HR-TEM images of the as-prepared [AP and APL₅] and their lattice fringes (c, d) and SAED images (e, f)



3.3.3 Optimum annealing conditions of APL₅ samples

Different batches of APL₅ samples were subjected to an isochronal annealing process for 1 h at four different temperatures, namely 300, 400, 500, and 550°C. Following that, the samples were exposed to 100 Gy of gamma dose and TL-intensity was recorded at a heating rate of 5 °C/s. Figure 5A reveals the glow curves of APL₅ samples prepared at various annealing temperatures, and Fig. 5B exhibits the TL-intensity representations of the data in Fig. 5A.

Fig. 2 continued

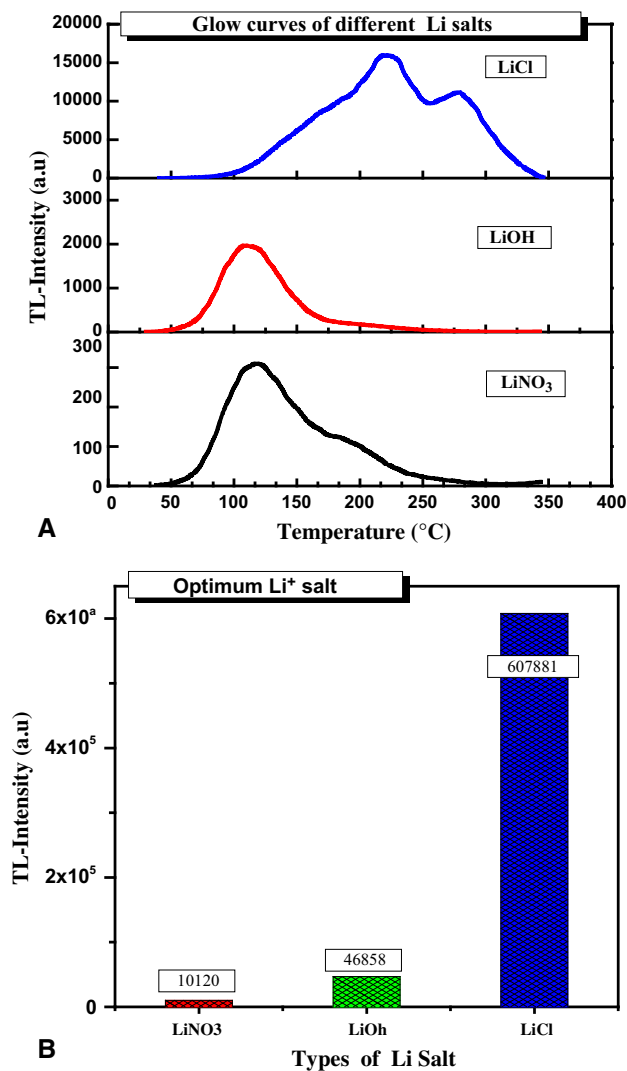


According to Fig. 5A and B, it can be concluded that the best (optimum) annealing condition is found to be at 500 °C for 1 h. In summary, the optimal preparation conditions of the presented new nanophosphor are based on the choice of (i) LiCl as co-host salt, (ii) 5 Wt% Li-concentrations, and (iii) annealing at 500 °C for 1 h. Ultimately, the APL₅ samples will be our best choice, as they have the better TL-response of any other samples.

3.3.4 Glow curve structure of APL₅ nanophosphor

The effect of gamma dose values on the glow curve of an APL₅ sample was studied within a dose range from 15 to 100 Gy, using 5 °C/s as a heating rate. Figure 6 depicts the variations of the TL-intensity with gamma doses where all the glow curves

Fig. 3 (A) TL- glow curves of $\text{Ag}_3\text{PO}_4:\text{Li}^+$ nanophosphors prepared with different Li co-host salt type, exposed to 100 Gy γ -doses and recorded at 5 °C/s (B) The dependence of TL intensity on the Li co-host salt type



are approximately similar in shapes and positions. This reflects the dependence of the number of induced trapping centers on the radiation dose values, where the trapped electrons increasing as the γ -dose values increase. Consequently, the TL intensity increases as the dose value goes up from 15 to 100 Gy.

3.3.5 TL-dose response of APL₅

The linearity relationship between the TL-intensity and the absorbed dose is one of the most important characteristics of any dosimeter. Figure 7 shows the dose–response relationship of sample APL₅ over a dose range of 15–100 Gy, demonstrating a linear response with a correlation coefficient of 0.9982. This behavior provides good performance when using such newly prepared phosphor materials in various fields of gamma radiation measurements within the studied dose range.

3.3.6 The minimum detectable dose (MDD)

The MDD is an estimated value that is useful in low dose measurements where the signal of the irradiated sample is very close to the background signal. It is also defined as the lowest dose or detection level that the sample can detect [38]. The MDD of the synthesized APL₅ nanophosphor was calculated using the empirical formula proposed by Furetta et al. [4, 38], which is given by

$$\text{MDD} = (\mathbf{B} + 2\sigma) \mathbf{F} \quad (1)$$

where (**B**) is the mean TL background signal obtained from the un-irradiated samples, (σ) is the standard deviation of the mean background, and (**F**) is the calibration factor, which can be determined from the linearity relationship (reciprocal of the slope) and

Fig. 4 (A) TL- glow curves of $\text{Ag}_3\text{PO}_4:\text{Li}^+$ of different Li-concentrations (1–7 wt%), exposed to 100 Gy γ -dose and readout at 5 °C/s (B) The variation of TL intensities with the Li-concentrations

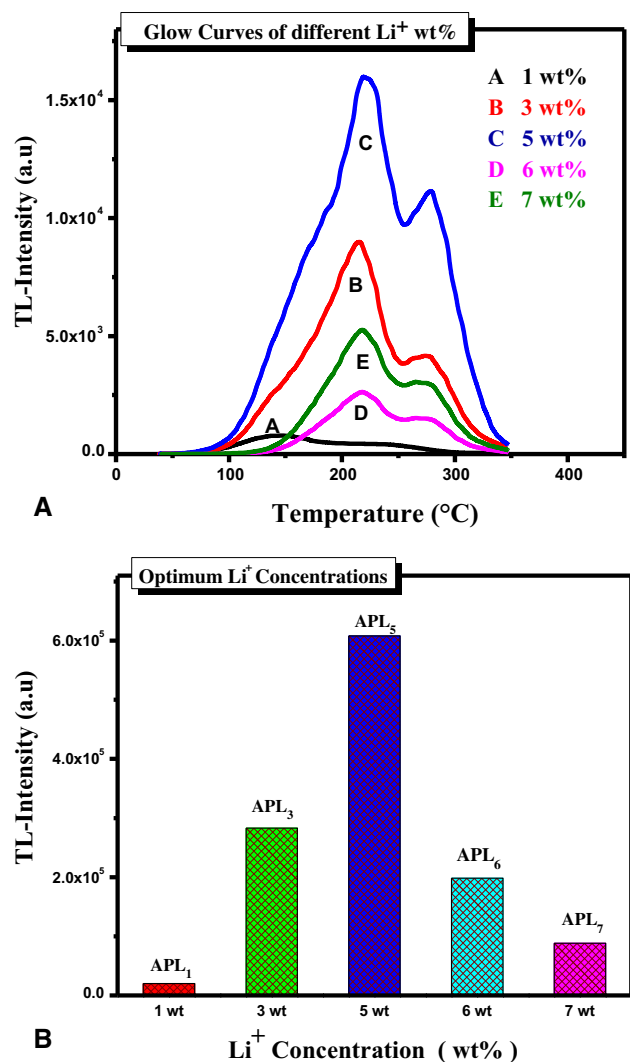


Table 1 TL-intensity of 10 batches from synthesized APL_5 nanophosphor

Batch No	1	2	3	4	5	6	7	8	9	10
TL-Intensity (a.u)	607,881	649,855	586,520	596,510	541,195	579,745	665,975	569,854	552,195	639,165

was found to be (0.177) mGy/nC . By substituting these values into Eq. (1), the MDD of the APL_5 sample was calculated to be around 5.149 mGy when the region of interest was used.

3.3.7 Batch size homogeneity (Δ) of nano APL_5 dosimeter

The International Electrochemical Commission (IEC) recommends that the evaluated value for any dosimeter in a batch not differ by more than 30% from any other dosimeter values in the same batch [39]. This was confirmed for the APL_5 nanophosphor sample under optimal conditions by exposing 100 mg of the sample to 100 Gy of γ -dose. The readouts of ten samples from the same irradiated batch are listed in Table 1.

From Table 1 the corresponding uniformity indices (Δ) are calculated using Eq. (2):

$$\Delta = (\mathbf{M}_{\max} - \mathbf{M}_{\min}) / \mathbf{M}_{\min} \times 100 \tag{2}$$

where \mathbf{M}_{\max} and \mathbf{M}_{\min} are the maximal and minimal recorded values, respectively. The uniformity indices value of the studied sample is then $\Delta = 23\%$, indicating the APL_5 nanophosphor sample homogeneity is within the IEC range.

Fig. 5 (A) TL-glow curves of $\text{Ag}_3\text{PO}_4:\text{Li}^+$ (5 wt% of LiCl) annealed at different temperatures (300–550 °C), exposed to 100 Gy γ -dose and readout at 5 °C/s (B) dependence of The TL- intensity on the annealing temperature

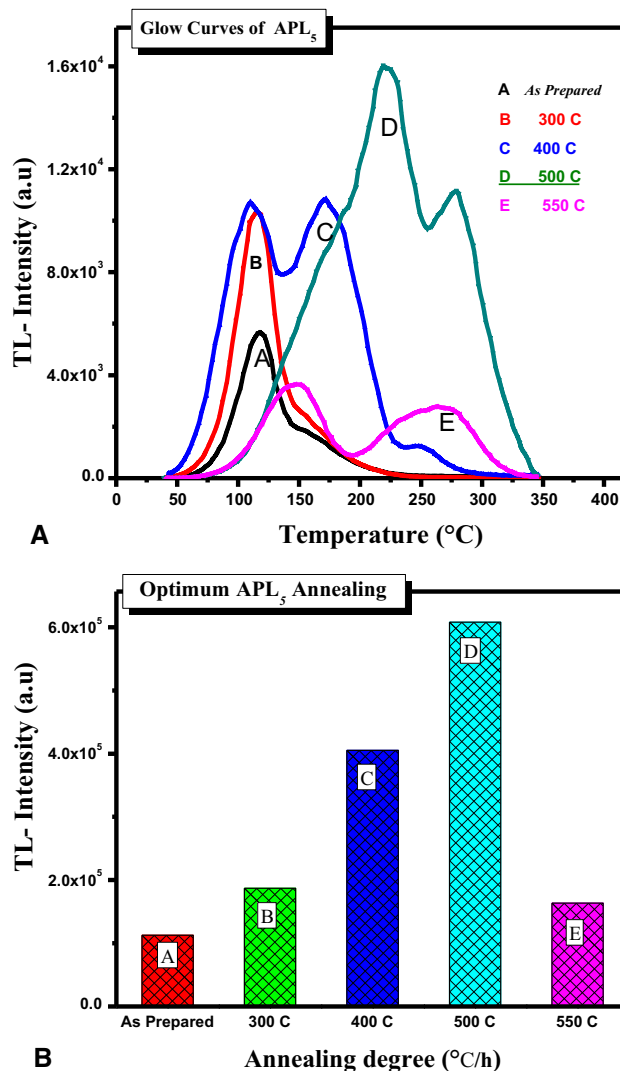


Fig. 6 TL-glow curves of the APL₅ nanophosphors at different gamma doses [15–100 Gy]

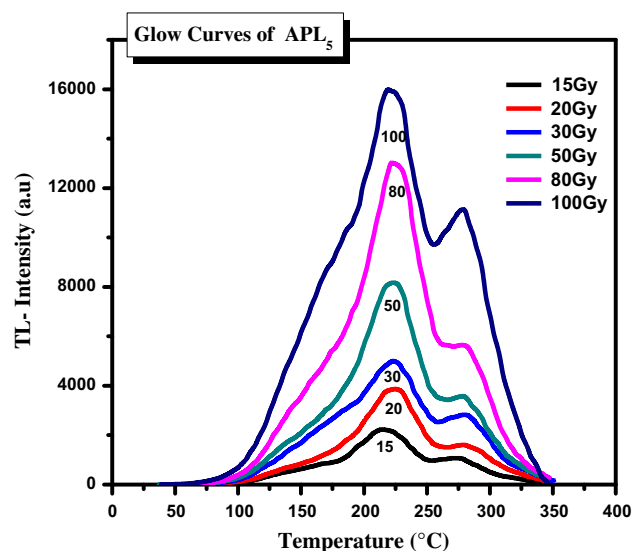


Fig. 7 TL-response of the APL₅ nanophosphors as a function of gamma doses

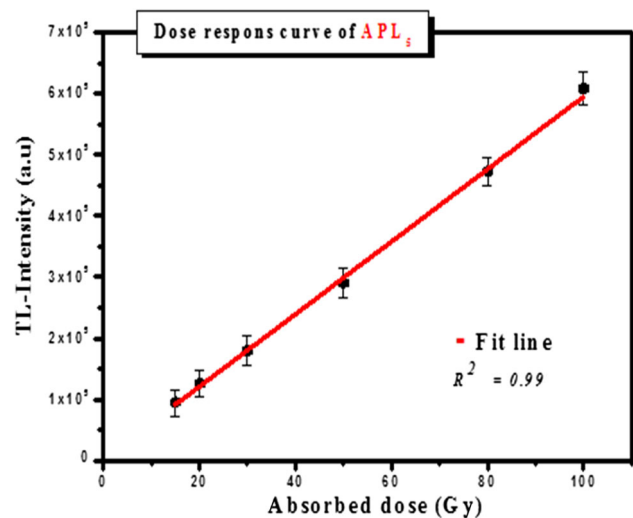
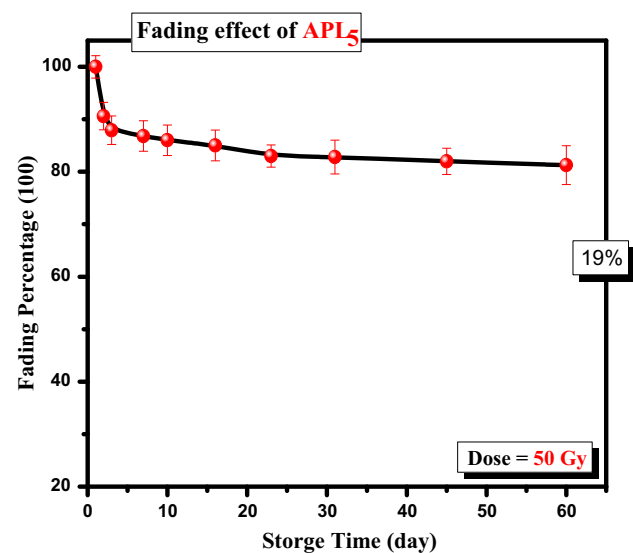


Fig. 8 Thermal fading curve of APL₅ nanophosphor after 50 Gy of γ -dose irradiation



3.3.8 Fading

Fading is an important parameter that should be determined before using any TLD. It represents the loss of the TL signal during the storage. The APL₅ phosphor samples were irradiated at 50 Gy of γ -doses, stored in the dark at room temperature for 60 days, and the TL was measured at various storage times. Every TL value was normalized to zero storage time.

Figure 8 depicts the relationship between fading percentage and storage time. According to Fig. 8, the TL signal losses of about 12%, 15%, and 19% were detected after times 3, 16, and 60 d, respectively. Following that, almost no losses were observed for storage times longer than 16 days. From a dosimetric standpoint, these fading results should be considered in the evaluation of corrected γ -dose.

4 Conclusions

A novel nanophosphor of Li⁺, with different concentrations, doped Ag₃PO₄ orthophosphate was synthesized by the coprecipitation method. The XRD and HR-TEM techniques were used to confirm the crystalline features and phase composition of AP and APL₅ nanomaterials with uniform sizes of about 10 and 15 nm, respectively. The TL properties of the synthesized nanophosphor showed that the sample doped with 5 Wt% of Li⁺ impurity (i.e., APL₅ sample) and thermally annealed at 500 °C for 1 h displayed the highest TL intensity among all the other compositions. The glow curves of irradiated APL₅ nanophosphors were recorded at a heating rate of 5 °C/s and revealed a simple structure with two glow peaks centered at approximately 222 and 279 °C. The TL characterizations of the APL₅ sample revealed a good linear TL response-gamma dose ($R^2 = 0.998$) over a range of 15 to 100 Gy with low fading and good

reproducibility. These excellent properties of the newly prepared APL₅ sample offered the preference of using this nanophosphor material in various photonic dosimetric applications within the studied γ -dose range.

Funding Open access funding provided by The Science, Technology & Innovation Funding Authority (STDF) in cooperation with The Egyptian Knowledge Bank (EKB).

Data availability statement The authors confirm that the data generated or analyzed during this study are included in this published article and its supplementary materials. This manuscript has data included as electronic supplementary material. The online version of this article contains supplementary material, which is available to authorized users

Open Access This article is licensed under a Creative Commons Attribution 4.0 International License, which permits use, sharing, adaptation, distribution and reproduction in any medium or format, as long as you give appropriate credit to the original author(s) and the source, provide a link to the Creative Commons licence, and indicate if changes were made. The images or other third party material in this article are included in the article's Creative Commons licence, unless indicated otherwise in a credit line to the material. If material is not included in the article's Creative Commons licence and your intended use is not permitted by statutory regulation or exceeds the permitted use, you will need to obtain permission directly from the copyright holder. To view a copy of this licence, visit <http://creativecommons.org/licenses/by/4.0/>.

References

1. S. McKeever, M. Moscovitch, On the advantages and disadvantages of optically stimulated luminescence dosimetry and thermoluminescence dosimetry. *Radiat Protect Dosimetry* (2003). <https://doi.org/10.1093/oxfordjournals.rpd.a006191>
2. T. Kron, Thermoluminescence dosimetry and its applications in medicine-Part1: Physics, materials and equipment, *Austr. Phys. Eng. Sci. Med.*, 17 (1994)
3. V. Kortov, Nanophosphors and outlooks for their use in ionizing radiation detection. *Radiat. Measur.* (2010). <https://doi.org/10.1016/j.radmeas.2009.11.009>
4. I. El-Mesady, S. Alawsh, H. Othman, A comparative dosimetric study between silicon activated aluminum-based nanocrystal and its corresponding glass system structure. *J. Luminesc.* (2020). <https://doi.org/10.1016/j.jlumin.2020.117555>
5. H. Hafez, E. Sheha, K. Abd-Elmageed, M. El-Kolaly, M. Sayed, The TL-properties of some environmental materials and assessment the effects of other different parameters. *SILICON* (2020). <https://doi.org/10.1007/s12633-019-00242-1>
6. H.A. Othman, H. Ammar, A. Hussein, H. El-Samman, S.A. Alawsh, I.A. El-Mesady, Structural and luminescent properties of aluminum-based nanophosphors. *Ceram. Int.* (2021). <https://doi.org/10.1016/j.ceramint.2021.06.206>
7. A. El-Adawy, N.E. Khaled, A.R. El-Sersy, A. Hussein, H. Donya, TL dosimetric properties of Li₂O–B₂O₃ glasses for gamma dosimetry. *Appl. Radiat. Isot.* (2010). <https://doi.org/10.1016/j.apradiso.2010.01.017>
8. I. El Mesady, S. Alawsh, Optical and luminescence properties of silicon doped alumino-phosphate-sodium glass system. *J. Non-Cryst. Solids* (2018). <https://doi.org/10.1016/j.jnoncrysol.2017.12.054>
9. N. Bajaj, C. Palan, K. Koparkar, M. Kulkarni, S. Omanwar, Preliminary results on effect of boron co-doping on CW-OSL and TL properties of LiMgPO₄: Tb, B. *J. Lumin.* (2016). <https://doi.org/10.1016/j.jlumin.2016.02.003>
10. J. Guo, L. Zhao, Q. Tang, C. Zhang, Y. Chen, Spectral study on energy transfer of the LiMgPO₄ phosphor doped with Tm³⁺ and Tb³⁺. *J. Lumin.* (2020). <https://doi.org/10.1016/j.jlumin.2020.117613>
11. S. More, M. Meshram, S. Wankhede, P. Muthal, S. Dhopte, S. Moharil, Luminescence in LiCaPO₄. *Physica B* (2011). <https://doi.org/10.1016/j.physb.2010.12.077>
12. A. Sahu, P. Chowdhary, V. Nayar, S. Dhoble, K. Dubey, Rare earth Dy activated Li₃PO₄: Dy phosphors for lyoluminescence dosimetry of ionizing radiations, *Recent Res. Sci. Technol.* (2012)
13. C. Palan, A. Chauhan, N. Sawala, N. Bajaj, S. Omanwar, Thermoluminescence and Optically Stimulated Luminescence Properties of MgB₄O₇:Ag Phosphor, *Int. J. Luminesc. Appl.* 5 (2015)
14. S. Menon, A. Singh, S. Kadam, S. Mhatre, B. Sanyal, B. Dhabekar, Dosimetric characterization of LiMgPO₄: Tb, B phosphor for its application in food irradiation. *J. Food Process. Preserv.* (2019). <https://doi.org/10.1111/jfpp.13891>
15. H. Tang, L. Lin, C. Zhang, Q. Tang, High-sensitivity and wide-linear-range thermoluminescence dosimeter LiMgPO₄:Tm, Tb, B for detecting high-dose radiation. *Inorg. Chem.* (2019). <https://doi.org/10.1021/acs.inorgchem.9b00597>
16. Z. Yi, J. Ye, N. Kikugawa, T. Kako, S. Ouyang, H. Stuart-Williams, H. Yang, J. Cao, W. Luo, Z. Li, An orthophosphate semiconductor with photooxidation properties under visible-light irradiation. *Nat. Mater.* (2010). <https://doi.org/10.1038/nmat2780>
17. L. Qin, P. Tao, X. Zhou, Q. Pang, C. Liang, K. Liu, X. Luo, Synthesis and characterization of high efficiency and stable spherical Ag₃PO₄ visible light photocatalyst for the degradation of methylene blue solutions. *J. Nanomater.* (2015). <https://doi.org/10.1155/2015/258342>
18. X. Li, P. Xu, M. Chen, G. Zeng, D. Wang, F. Chen, W. Tang, C. Chen, C. Zhang, X. Tan, Application of silver phosphate-based photocatalysts: Barriers and solutions. *Chem. Eng. J.* (2019). <https://doi.org/10.1016/j.cej.2019.02.083>
19. K. Zhong, J. Su, Study on the visible-light photocatalytic performance of Ag₃PO₄/Cu₂O composite. *Res. Chem. Intermed.* (2019). <https://doi.org/10.1007/s11164-018-3662-z>
20. D.A. Septiarini, M. Kurniasih, R. Andreas, D. Hermawan, U. Sulaeman, Synthesis of silver orthophosphate under dimethyl sulfoxide solvent and their photocatalytic properties, *IOP Conference Series: Materials Science and Engineering*. IOP Publishing (2019). <https://doi.org/10.1088/1757-899X/509/1/012151>
21. G. Hou, X. Zeng, S. Gao, Fabrication and photocatalytic activity of core@ shell Ag₃PO₄@ Cu₂O heterojunction. *Mater. Lett.* (2019). <https://doi.org/10.1016/j.matlet.2018.11.170>
22. G. He, W. Yang, W. Zheng, L. Gong, X. Wang, Y. An, M. Tian, Facile controlled synthesis of Ag₃PO₄ with various morphologies for enhanced photocatalytic oxygen evolution from water splitting. *RSC Adv.* (2019). <https://doi.org/10.1039/C9RA01306G>
23. M. Afif, U. Sulaeman, A. Riapanitra, R. Andreas, S. Yin, Use of Mn doping to suppress defect sites in Ag₃PO₄: Applications in photocatalysis. *Appl. Surf. Sci.* (2019). <https://doi.org/10.1016/j.apsusc.2018.10.049>
24. X. Zhao, L. Song, S. Zhang, Synthesis of AgCl/Ag₃PO₄ composite photocatalysts and study on photodegradation activity based on a continuous reactor. *Photochem. Photobiol.* (2018). <https://doi.org/10.1111/php.12875>

25. M. Kalinkin, M.Y. Yanchenko, L.Y. Buldakova, A. Dmitriev, N. Zhuravlev, D. Kellerman, Photocatalytic activity of LiMgPO_4 in the hydroquinone decomposition and related surface phenomena, *Reaction Kinetics. Mechanisms and Catalysis* (2020). <https://doi.org/10.1007/s11144-020-01754-3>
26. P. Sahare, M. Singh, P. Kumar, TL characteristics of Ce^{3+} -doped NaLi_2PO_4 TLD phosphor. *J. Radioanal. Nucl. Chem.* (2014). <https://doi.org/10.1007/s10967-014-3273-0>
27. K. Huang, Y. Lv, W. Zhang, S. Sun, B. Yang, F. Chi, S. Ran, X. Liu, One-step synthesis of $\text{Ag}_3\text{PO}_4/\text{Ag}$ photocatalyst with visible-light photocatalytic activity. *Mater. Res.* (2015). <https://doi.org/10.1590/1516-1439.346614>
28. I. Bozetine, Y. Boukennous, M. Trari, N. Moudir, Synthesis and characterization of orthophosphate silver powders. *Energy Procedia* (2013). <https://doi.org/10.1016/j.egypro.2013.07.131>
29. A. El-Adawy, A. Hussein, E. R. Sheha, S. Abdel-Samad, Ahmad A. Hassan, and M. Al-Abyad, Synthesis and Thermoluminescence of Novel $\text{Ag}_3\text{PO}_4:\text{Ba}^{2+}$ Nanophosphor as Gamma Radiations Detector. (2021). <https://doi.org/10.21608/ejchem.2021.62097.3335>
30. P. Amornpitoksuk, K. Intarasuwan, S. Suwanboon, J. Baltrusaitis, Effect of phosphate salts (Na_3PO_4 , Na_2HPO_4 , and NaH_2PO_4) on Ag_3PO_4 morphology for photocatalytic dye degradation under visible light and toxicity of the degraded dye products. *Ind. Eng. Chem. Res.* (2013). <https://doi.org/10.1021/ie401821w>
31. X. Song, R. Li, M. Xiang, S. Hong, K. Yao, Y. Huang, Morphology and photodegradation performance of Ag_3PO_4 prepared by $(\text{NH}_4)_3\text{PO}_4$, $(\text{NH}_4)_2\text{HPO}_4$ and $\text{NH}_4\text{H}_2\text{PO}_4$. *Ceram. Int.* (2017). <https://doi.org/10.1016/j.ceramint.2016.12.124>
32. G. Ju, Y. Hu, L. Chen, X. Wang, Z. Mu, Concentration quenching of persistent luminescence. *Physica B* (2013). <https://doi.org/10.1016/j.physb.2013.01.027>
33. <https://www.scribd.com/document/444219253/XRD-Introduction-to-XPert-Pro-pdf>.
34. S. A. Speakman. Introduction to x-ray powder diffraction data analysis. Center for Materials Science and Engineering at MIT (2013)
35. B. Voutou Electron Microscopy: The Basics. *Physics of Advanced Materials Winter School 1*, No. 11 (2008)
36. Murthy, et al. "Thermoluminescence: Basic Theory, Applications and Experiments, Published By Nucleonix Systems Pvt." Ltd., Hyderabad, India (2008)
37. L. Wang, Z. Dai, R. Zhou, B. Qu, X.C. Zeng, Understanding the quenching nature of Mn^{4+} in wide band gap inorganic compounds: design principles for Mn^{4+} phosphors with higher efficiency. *Phys. Chem. Chem. Phys.* (2018). <https://doi.org/10.1039/C8CP02569J>
38. M. Sabry, H.A. Alazab, A. Gad, N. El-Faramawy, Thermoluminescence properties of natural Egyptian calcite. *J. Lumin.* **238**, 118273 (2021). <https://doi.org/10.1016/j.jlumin.2021.118273>
39. J. Stefanik, Thermoluminescence dosimetry systems for personal and environmental monitoring (International Electrotechnical Commission Standard Publication 61066: 1991), (2000)